

## Significantly enhanced giant Rashba splitting in a thin film of binary alloy

This content has been downloaded from IOPscience. Please scroll down to see the full text.

2015 New J. Phys. 17 083015

(<http://iopscience.iop.org/1367-2630/17/8/083015>)

View [the table of contents for this issue](#), or go to the [journal homepage](#) for more

Download details:

IP Address: 140.109.101.40

This content was downloaded on 07/08/2015 at 04:14

Please note that [terms and conditions apply](#).



## PAPER

## Significantly enhanced giant Rashba splitting in a thin film of binary alloy

## OPEN ACCESS

## RECEIVED

11 March 2015

## REVISED

21 June 2015

## ACCEPTED FOR PUBLICATION

23 June 2015

## PUBLISHED

6 August 2015

Content from this work  
may be used under the  
terms of the [Creative  
Commons Attribution 3.0  
licence](#).

Any further distribution of  
this work must maintain  
attribution to the  
author(s) and the title of  
the work, journal citation  
and DOI.



Wei-Chuan Chen<sup>1,2,6</sup>, Tay-Rong Chang<sup>1,6</sup>, Sun-Ting Tai<sup>1</sup>, S Yamamoto<sup>3</sup>, Je-Ming Kuo<sup>1,2</sup>,  
Cheng-Maw Cheng<sup>2</sup>, Ku-Ding Tsuei<sup>1,2</sup>, Koichiro Yaji<sup>3</sup>, Hsin Lin<sup>4</sup>, H-T Jeng<sup>1,5</sup>, Chung-Yu Mou<sup>1</sup>,  
Iwao Matsuda<sup>3</sup> and S-J Tang<sup>1,2</sup>

<sup>1</sup> Department of Physics, National Tsing Hua University, Hsinchu, Taiwan 30013

<sup>2</sup> National Synchrotron Radiation Research Center (NSRRC), Hsinchu, Taiwan 30076

<sup>3</sup> Institute for Solid State Physics, the University of Tokyo, 5-1-5 Kashiwanoha, Kashiwa, Chiba 277-8581, Japan

<sup>4</sup> Graphene Research Centre and Department of Physics, National University of Singapore, Singapore 117542

<sup>5</sup> Institute of Physics, Academia Sinica, Taipei, Taiwan 11529

<sup>6</sup> Authors contributed equally to the paper.

E-mail: [sjtang@phys.nthu.edu.tw](mailto:sjtang@phys.nthu.edu.tw)

**Keywords:** giant Rashba splitting, binary alloy, Pb and Au

Supplementary material for this article is available [online](#)

## Abstract

Dirac cones in a two-dimensional environment have attracted much attention not only because of the massless Dirac fermions but also due to their capability to lock the spin direction with the momentum. Here we demonstrate that the Rashba effect within a single layer of a binary alloy composed of heavy atoms, Pb and Au, can be driven by and even tweaked with the adjacent top and bottom layers to yield cone-like structures and further enhance the Rashba coupling strength. Two cones are observed at the surface zone center  $\bar{\Gamma}$  with giant Rashba parameters 1.53 and 4.45 eVÅ; an anisotropic giant Rashba splitting at the surface zone boundary  $\bar{M}$  has a great value, 6.26 eVÅ, inferring the critical role of  $p$ - $d$  hybridization between Pb and Au. Our results reveal not only an interesting natural phenomenon but also a feasible method of tweaking the Rashba effect of a two-dimensional system.

## 1. Introduction

Spin-orbit coupling (SOC) is an atomic property caused by the electric field exerted on an electron from a nucleus. The electric field relativistically becomes the magnetic field and removes the degeneracy of the electron energy levels due to the intrinsic spin of an electron. An interface between a vacuum and a solid would typically break the inversion symmetry and cause further splitting, so-called Rashba splitting [1], with time-reversal symmetry preserved. SOC is proportional to the square of the charge,  $Z^2$ , of a nucleus; a surface terminated on a heavy-element solid is hence expected to exhibit a Rashba effect via splitting of two-dimensional (2D) surface states [2–4]. Another way to produce the Rashba effect is to form an ultra-thin layer of a heavy element on a semiconductor surface [5–9]. Moreover, Ast *et al* [10] formed a thin BiAg-alloy layer on a Ag(111) crystal surface and observed a giant Rashba spin splitting that was attributed to the in-plane potential gradient as opposed to the out-of-plane gradient of a typical Rashba picture. A PbAg-alloy layer on Ag(111) was observed to exhibit smaller Rashba spin splitting [11]. First-principles calculations on both alloys attributed the enhancement of the Rashba effect to the strong distortion of the surface-state wave function [12]. Both alloy films comprise heavy and light atoms to produce the in-plane electric field; however, more accurately, it is more related to how electrons are distributed in vicinity of atomic cores of heavy atoms than to types of atoms involved. Interesting physics might arise in such a system where strong potential gradients are possible in both in-plane and out-of-plane directions. In addition, the Rashba effect has been considered to be orbital dependent [12, 13]. Additional types of angular-momentum orbitals such as  $d$  and  $f$  may participate in the hybridization between two composite heavier elements, hence causing the asymmetry of the wavefunction for the mixed orbitals, which has also been considered a crucial factor for the Rashba effect [13, 14]. We have generated thin

films of binary alloy of heavy-metal atoms, PbAu alloy, on Pb films grown on Ge(111). The similar PbAu alloys were formed on Pb films grown on Si(111) and studied microscopically [15, 16]. However, the focus was on the morphologies, lattice structures, and stoichiometric composition. No attempts to study the electronic structures were made. Pb films can grow atomically uniform on both Ge(111) and Si(111) [17, 18] and we chose Ge(111) as the bottom substrate for our study. Using angle- and spin-resolved photoemission spectra and low-energy electron diffraction (LEED), we measured the electronic, spin, and lattice structures of these thin films. Two spin-polarized cone-like electronic structures were observed at the surface zone center; one is derived mainly from Pb *sp* orbitals, and the other is derived partially from Au *s* and *d* orbitals. The lattice of the alloy thin film exhibits a structure near  $\sqrt{3} \times \sqrt{3}$  R30° with respect to the underlying Pb(111)- $1 \times 1$  film; however, first-principles calculations of the electronic structure indicate similar cone-like structures only when the alloy film is covered with one Au layer to induce a special buckling configuration of the alloy film, which breaks the inversion symmetry.

## 2. Methods

### 2.1. Experimental details

The angle-resolved photoemission spectra were measured at room temperature with photons of energy 21.2 eV from a He lamp (unpolarized) and synchrotron radiation (*p*-polarized) from undulator beamline 21B1-U9 at the National Synchrotron Radiation Research Center in Taiwan. The spin-resolved photoemission spectra were measured at the BL-19A undulator beamline in the KEK-Photon Factory. The energy resolution of the spectra is 50 meV, and the angular resolution is  $\pm 1^\circ$ . The spectrometer was equipped with a new high-yield spin detector that has an electron-exchange interaction with excited photoelectrons through very low-energy electron diffraction (VLEED) of electrons at a ferromagnetic target Ni, with effective Sherman function  $S_{\text{eff}} = 0.35$ . Two different methods are used to grow PbAu alloy in this study; PbAu alloy on Pb films and Pb Au alloy on a Pb(111) bulk crystal surface. For the former, Ge(111) wafers that were *n*-type doped were selected as substrates. Via standard sputtering and annealing, clean surfaces of Ge(111)- $c(2 \times 8)$  were obtained. To form the structure Au/Ge(111)- $\sqrt{3} \times \sqrt{3}$  R30°, we deposited a Au film (3–6 Å); the substrate was subsequently annealed from 296 K to 873 K. An overlayer uniform Pb film was formed by depositing Pb onto the structure Au/Ge(111)- $\sqrt{3} \times \sqrt{3}$  R30° maintained at 143 K. For the latter, a clean Pb(111) crystal surface was obtained by cycles of sputtering at room temperature and subsequent annealing at 473 K. The subsequent growth of the PbAu alloy is described in the main text.

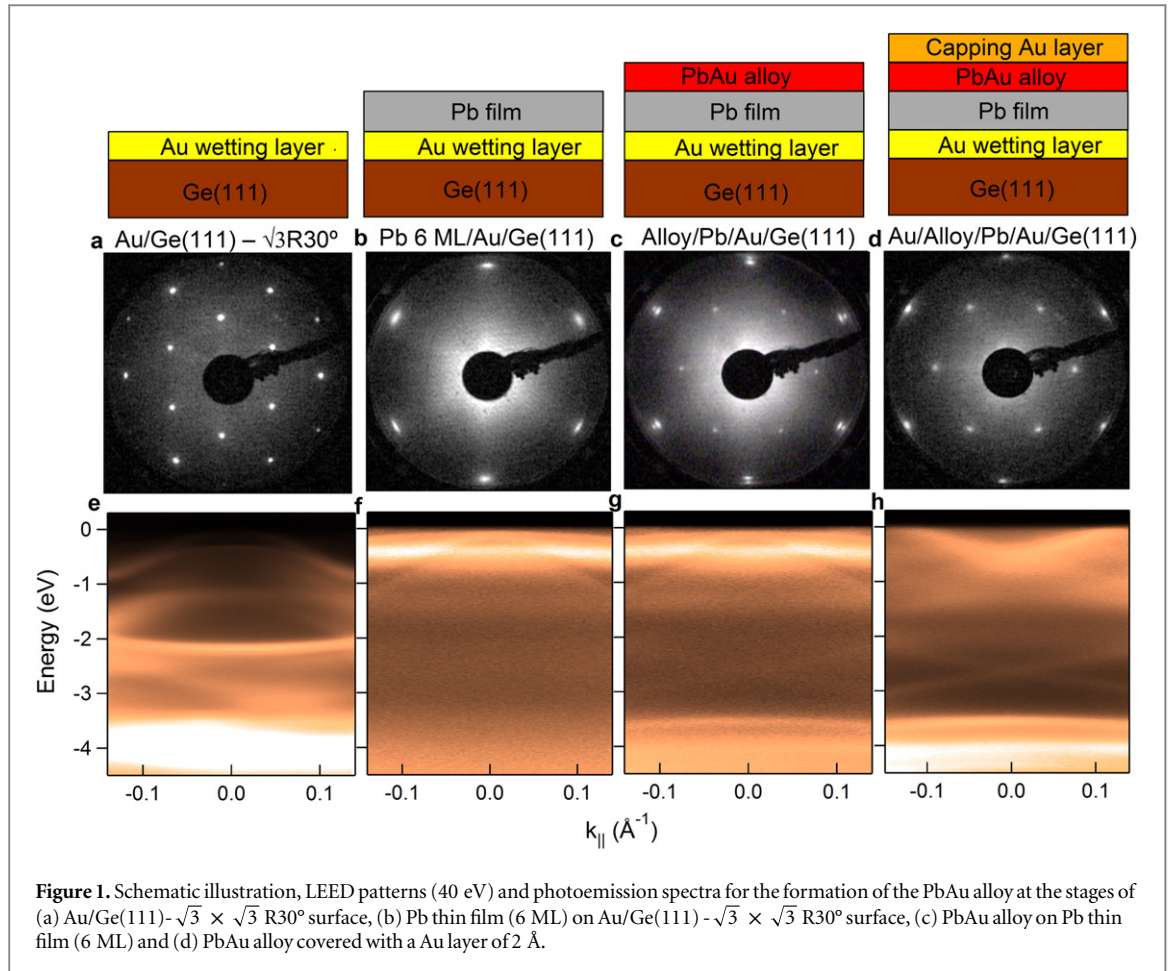
### 2.2. Theoretical details

The first-principles calculations were performed based on the generalized gradient approximation (GGA) [19] using the projector augmented-wave method [20] as implemented in the VASP package [21]. Slabs with vacuum thicknesses larger than 20 Å were used, satisfactorily separating the slabs. We used the slab model of Au/Pb<sub>2</sub>Au/Pb(111), as shown in figure 5(a), to determine the relaxed atomic positions, but a simplified model (Pb<sub>2</sub>Au single layer) for the band structures. The experimental lattice constant (5.7 Å) was used for the calculation. We fixed the Pb atoms of the bottom layers and relaxed the other atoms until the residual forces were less than 0.01 eV Å<sup>-1</sup>. The SOC was included self-consistently in the electronic structure calculation with a  $12 \times 12 \times 1$  Monkhorst-Pack *k*-point mesh.

## 3. Results and discussions

### 3.1. Stages for the formation of PbAu alloys on Pb films

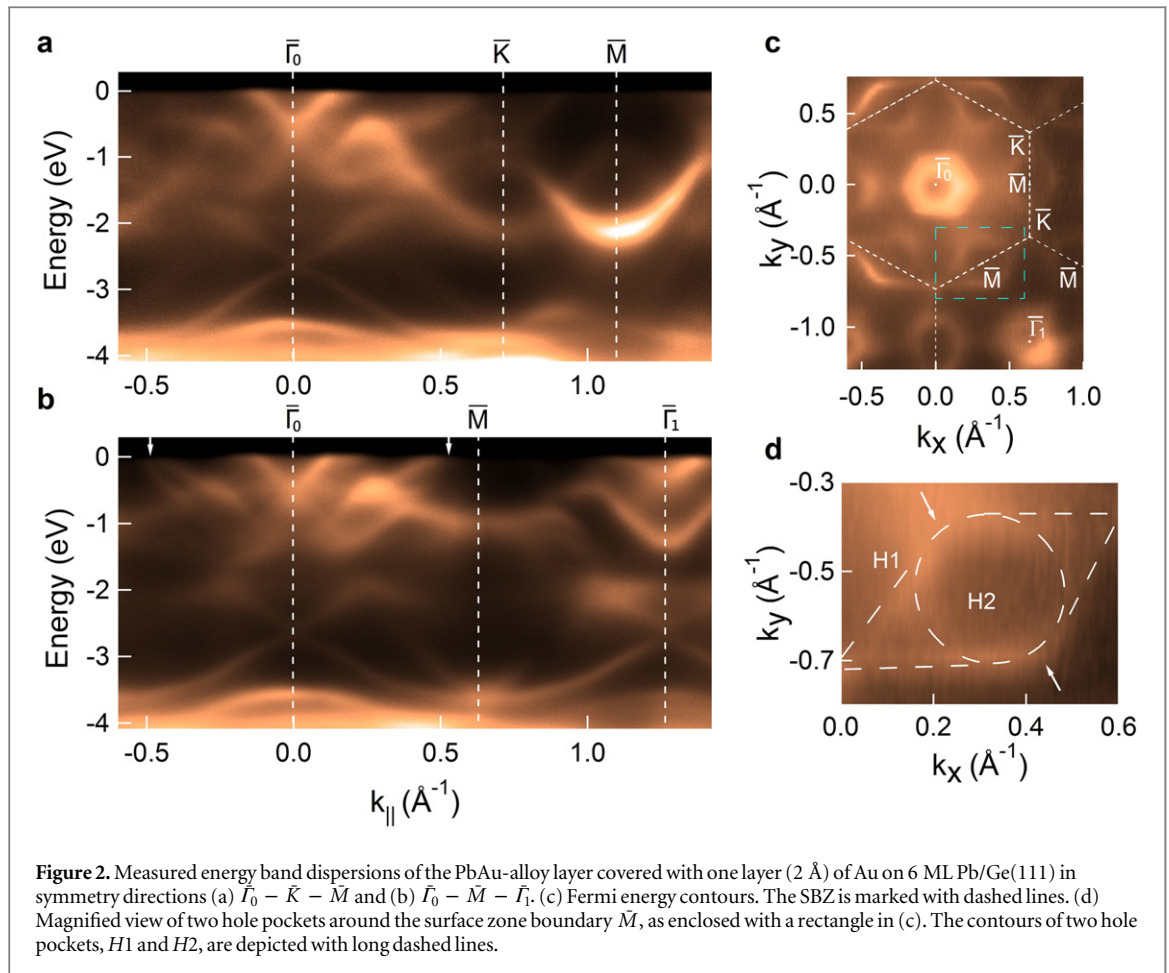
This PbAu alloy on Pb thin film was grown in a unique manner, as shown schematically in the top panel of figure 1. First, we prepared a wetting layer Au/Ge(111)- $\sqrt{3} \times \sqrt{3}$  R30° and then deposited Pb films on top of this layer at 143 K. The Pb films were subsequently annealed mildly at 296 K. Then, additional deposition of Au atoms onto the Pb films after annealing was required to obtain a PbAu-alloy phase. Finally excessive Au atoms form as the capping layer on top of the PbAu alloy. The middle panels of figures 1(a)–(d), show the LEED patterns in series of Au/Ge(111)- $\sqrt{3} \times \sqrt{3}$  R30°, 6 ML Pb(111) film, and subsequent deposition of Au onto the Pb(111) films. Figure 1(b) reveals that the lattice of the 6 ML Pb(111) film exhibits a hexagonal structure  $1 \times 1$  on top of the wetting layer Au/Ge(111)- $\sqrt{3} \times \sqrt{3}$  R30°, distinct from the case of Pb films on Pb/Ge(111)- $\sqrt{3} \times \sqrt{3}$  R30° for which incommensurate  $1 \times 1$  and commensurate  $\sqrt{3}$  phases coexist [17]. Figure 1(c) presents a LEED pattern of the PbAu alloy that exhibits a rotation by 30° with respect to Pb(111); however, its lattice is incommensurate with Pb(111)- $\sqrt{3} \times \sqrt{3}$  R30°, as revealed by the (2/3, 2/3) spots that exhibit splitting. The inner and outer components of the doublets originate from the underlying Pb(111) film and the alloy film, respectively. This behavior was observed by Yu *et al*, who deposited Au on Pb films grown on Si(111) [15]; these



researchers attributed this splitting to the lattice mismatch of  $\sim 2\%$  between the in-plane lattices of the PbAu alloy (5.7 Å) and Pb(111)- $\sqrt{3} \times \sqrt{3}$  R30° (6.06 Å). Their further investigation indicated that excess Au atoms form a capping Au layer,  $\sqrt{3} \times \sqrt{3}$ -Au, consistent with our result in figure 1(d), in which the LEED spots remain the same except for those that vanish from the underlying Pb films after further Au atoms (2 Å) are deposited. However, the Moiré patterns were clearly observed in microscopic images [15, 16] to reflect the strain effects from the top  $\sqrt{3} \times \sqrt{3}$ -Au and the bottom Pb(111) film to the middle PbAu alloy. The disparate strains from the top Au layer and the bottom Pb layers are perceived to cause this middle PbAu-alloy layer to possess a special outward relaxation or buckled configuration that is strongly tied to the Rashba coupling strength according to previous investigations on BiAg alloys [11, 22, 23]. The bottom panels in figures 1(e)–(h) show the corresponding photoemission spectra around  $\bar{\Gamma}_0$  for each stage. At the stage of Au/Ge(111)- $\sqrt{3} \times \sqrt{3}$  R30°, the downward hole-like Ge bulk bands disperse from the valence maximum at  $\bar{\Gamma}_0$  near the Fermi level [24], and the intense Au *d* flat bands around -4.0 eV were observed in addition to an upward surface-state band at -2.17 eV [25]. Then for the 6 ML Pb film on top of it, those features vanish; instead, one observed the flat quantum-well-state band of Pb films dispersing at -0.41 eV. Such kind of quantum-well-state band with large effective mass was attributed to the interaction with semiconductor hole bands [26] and electron localization [27]. As the single PbAu-alloy layer forms, the intensity of the quantum-well-state band starts decreasing and at about -3.50 eV, a slightly downward *d*-like band appears. Moreover, when the excessive Au atoms of 2 Å are deposited on top of the alloy, two cone-like structures with linear dispersions emerge.

### 3.2. Photoemission results for PbAu alloys on Pb films

Figures 2(a) and (b) show the energy band dispersions of the PbAu alloy covered with one-layer (2 Å) Au in two symmetry directions,  $\bar{\Gamma}_0 - \bar{K} - \bar{M}$  and  $\bar{\Gamma}_0 - \bar{M} - \bar{\Gamma}_1$ , in terms of the surface Brillouin zone (SBZ) of the alloy, constructed via the LEED spots in figure 1(d). Two cone-like band structures with linear dispersions are observed to cross at -0.56 eV and -2.65 eV respectively, at the surface zone center  $\bar{\Gamma}_0$ . The top cone crosses  $E_F$  at  $k_{\parallel} = \pm 0.13 \text{ \AA}^{-1}$ , whereas the bottom cone exhibits an elongated dispersion; in particular, in the symmetry direction  $\bar{\Gamma}_0 - \bar{M} - \bar{\Gamma}_1$ , the bottom cone band crosses the first SBZ to the surface zone boundary  $\bar{M}$  at -3.60 eV and then  $\bar{\Gamma}_1$  in the second one, forming the next bottom cone. However, the binding energy and Fermi vector of the top cone substantially decreased at  $\bar{\Gamma}_1$ . The extracted constant group velocities,  $v = \hbar^{-1} \nabla_k E(k)$ , of these two



cones are  $6.55 \times 10^5 \text{ m s}^{-1}$  and  $3.39 \times 10^5 \text{ m s}^{-1}$ , respectively, which are compatible with the values measured for topological insulators (TIs) [28] and graphene [29]. Figure 2(c) shows the Fermi energy contours of the alloy with the corresponding SBZ and symmetry momentum points superimposed. The top cone, an inherent electron pocket, constitutes therein a hexagonal contour around the surface zone center. In contrast, contours of an oval shape surround the surface zone boundary  $\bar{M}$ ; these contours are derived from two hole pockets ( $H1$ ,  $H2$ ), as indicated by the arrows in figure 2(b), in which two adjacent bands merge at  $E_F$  toward  $\bar{M}$ . The magnified view in figure 2(d) shows that the Fermi contours of the hole pockets around  $\bar{M}$  form two concentric oval contours that coincide at points (indicated by arrows) corresponding to the merging points of  $H1$  and  $H2$  at  $E_F$  in figure 2(b). The outer oval is, however, more rhombohedral.

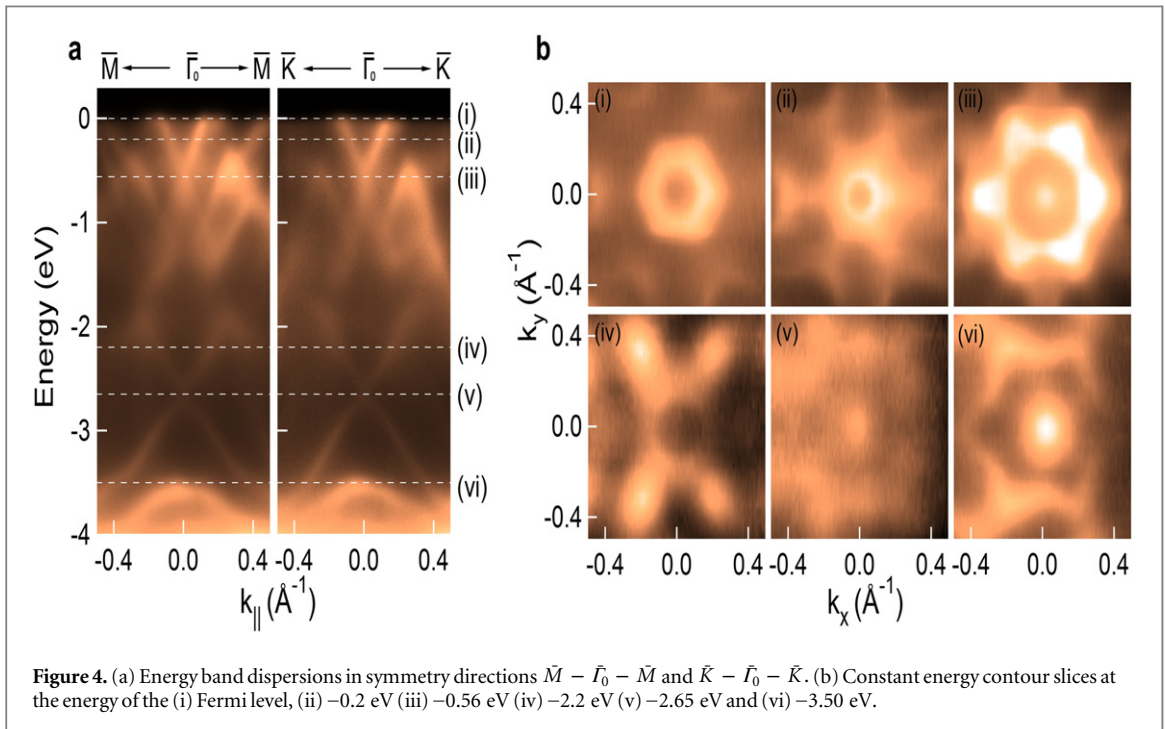
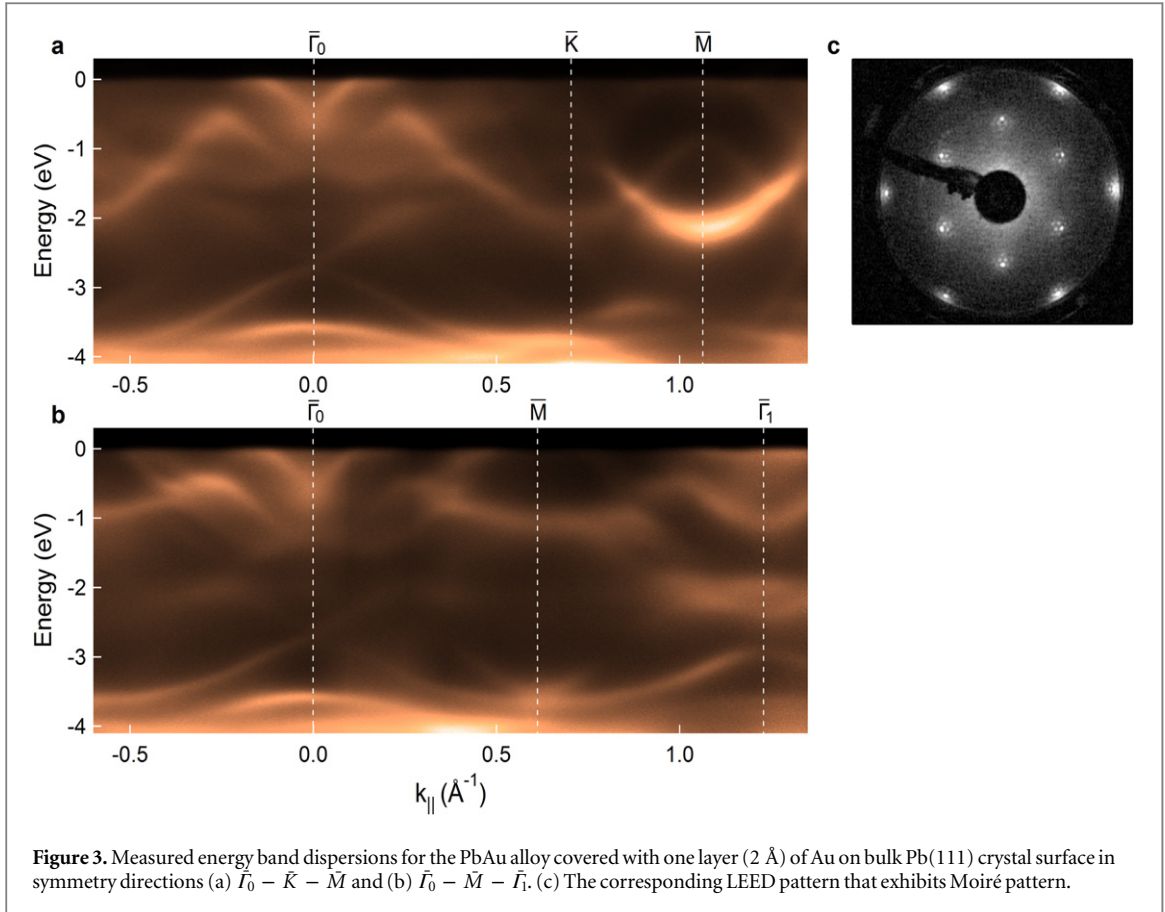
### 3.3. Comparison with the PbAu alloy on the Pb(111) crystal

Before proceeding into further investigation of the unique electronic structures of this alloy, clarification is needed to make sure of the role of the bottom substrate, Ge(111). Figures 3(a) and (b) present the corresponding energy band structures of PbAu alloy capped with a 2 Å Au layer on top of a bulk Pb(111) crystal surface. As observed, the energy band structures resemble those in figures 2(a) and (b) in spite of intensity variation. However, the LEED pattern, shown in figure 3(c), is more pronounced in the sense that it exhibits satellite Moiré spots around each alloy spot. Such Moiré patterns were observed from previous microscopic study [15, 16]. Therefore, we argue that the Ge(111) substrate and even the quantum well states of Pb films are not relevant to the unique electronic structures of PbAu alloy we observe. It also confirms that these unique electronic structures are not the consequence of Umklapp scattering of Pb electronic states since the electronic structures of Pb films and bulk Pb are distinct<sup>7</sup>.

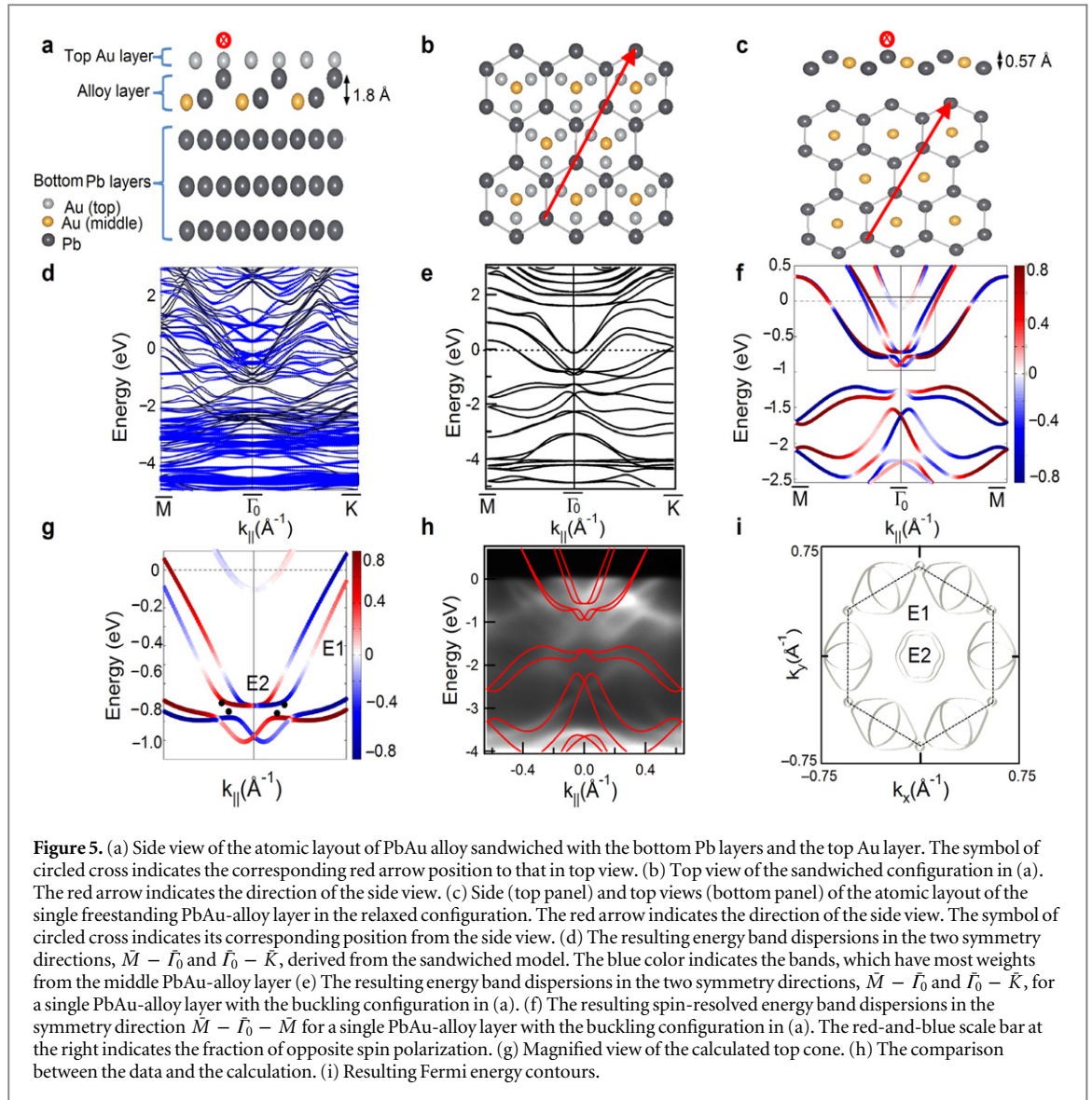
### 3.4. Constant energy contours

Figure 4 exhibits 2D slices of constant energy contours as a function of energy. From  $E_F$  to increasing binding energies, the hexagonal contour of the top cone converges to a point at an energy of  $-0.56 \text{ eV}$ . The bottom cone

<sup>7</sup> In the supplementary material (available at [stacks.iop.org/njp/17/083015/mmedia](http://stacks.iop.org/njp/17/083015/mmedia)), the measured energy band structures of 6M-Pb film and Pb(111) bulk crystal are displayed.



spans an energy range from -1.86 eV to -3.63 eV. The upper half (-1.86 eV to -2.65 eV) exhibits a quasi-circular shape, which is not clearly resolved because of interference from other bands. But below the convergence at -2.65 eV the lower half exhibits a clearly snowflake-shaped contour, which is typically observed in a TI material of rhombohedral/trigonal structure due to the hexagonal warping term for the spin-orbit interaction at the surface with three-fold symmetry [30]. At energy -3.50 eV another contour appears within the



bottom-cone contour, which stems from the downward energy band below the bottom cone that has a strong *d* character of Au.

### 3.5. The calculation model and results and comparison with data

Figure 5(a) shows a side view of the atomic-model layout of this PbAu alloy, which we employ for the calculation of the electronic structure; this arrangement follows an indication from the LEED results presented in figures 1(b)–(d). Three Pb(111) layers, represented by dark balls, serve as a base of the PbAu alloy. However, the in-plane lattice of Pb(111) is intentionally decreased from 3.50 Å to 3.29 Å to become commensurate with that of the alloy; a large unit cell involving numerous atoms is otherwise required, exceeding the computing capabilities. Figure 5(b) presents the corresponding top view of the lattice structure of the sandwiched model for PbAu alloy in the relaxed form. The Pb:Au ratio of the middle PbAu-alloy layer is 2:1 according to the preceding results [15, 16]. The centered Au atom, represented by the gold ball, of each hexagonal unit corresponds to the alloy structure  $\sqrt{3} \times \sqrt{3}$  R30° (5.7 Å) observed with LEED. The top capping Au layer, represented by gray balls, is commensurate with the middle PbAu alloy but via a Kagome structure, as shown in figure 5(b); the top Au atoms (gray balls) form as trimers centered at the Au atoms (gold balls) of the middle alloy layer to form a stable configuration with minimum energy according to the calculation. This Kagome structure of the Au layer was proposed for the 2D layer stacking, AuPb<sub>2</sub>/Au/AuPb<sub>2</sub>/Au/..., of the bulk PbAu-alloy crystal in the [111] direction [31]. In addition, similar trimer structure was also proposed by Qi *et al* [16] for their lattice-structure model of PbAu-alloy layers on Pb films grown on Si(111). Notably, the side views of both a freestanding alloy (top panel of figure 5(c)) and a sandwiched alloy (figure 5(b)) exhibit a great contrast in buckling configuration, in which the inversion symmetry is maintained for the former but not for the latter, consequently leading to

substantially altered electronic structures of the alloy. In addition, the buckling height that was observed to be closely related to the Rashba effect [12, 22, 23] also greatly increases from 0.57 Å to 1.80 Å from the former to the latter. As a reference, the measured and calculated buckling heights of BiAg- and PbAg-alloy layers are similar to that of the freestanding PbAu alloy [23]. Figure 5(d) displays calculated energy band structures in two major symmetry directions extracted from the sandwiched model in figure 5(a), which appear complicated even for the part having the most weight from the middle alloy layer, indicated by the blue color. To simplify and facilitate the comparison between the data and the calculation result, instead, we obtained the calculated energy band structures from one single alloy layer but with the same buckling configuration as that of the sandwiched one. Figure 5(e) shows the corresponding calculated dispersions of this simplified model in the same two symmetry directions. Based on this, we further adjusted the Fermi level position to make the calculated Fermi energy contours consistent with the measured ones in figure 2(c). Figure 5(f) presents the corresponding calculated dispersions of the spin-resolved energy bands of the PbAu alloy in the symmetry directions,  $\bar{M} - \bar{\Gamma}_0 - \bar{M}$  after this adjustment. The red and blue colors indicate opposite in-plane spin directions. As observed, the calculated top cone at  $\sim -0.89$  eV comprises one pair of Rashba spin-splitting bands anticrossing one pair of nearly spin-degenerate flat bands that turn upward with increasing  $k_{\parallel}$  and cross  $E_F$ , forming hole pockets around  $\bar{M}$ . Because of this anticrossing, the original Rashba-splitting bands are divided into two spin-polarized bands—a deeper band ( $E1$ ) and a shallower one ( $E2$ ), as depicted in the magnified view in figure 5(g). We hence reasonably argue that the observed top cones at  $\bar{\Gamma}_0$  of the first and at  $\bar{\Gamma}_1$  of the second SBZ in figure 2(b) correspond to  $E1$  and  $E2$ , respectively, which must have opposite parities in orbital symmetry with respect to a particular mirror plane such that the magnitudes of the photoemission matrix elements for these cones differ with a specific polarization of the beam. A similar behavior was observed in the photoemission spectra of iron-based high-temperature superconductors [32, 33], in which the replica of bands invariably possessed a parity switching of their orbital characters across the boundary of the Brillouin zone because translational symmetry was suppressed. According to a fit of the  $E1$  and  $E2$  bands in the measured spectra via Rashba-splitting and anticrossing models, the extracted value of the Rashba parameter of the top cone is 1.53 eV Å. The calculated bottom cone is at  $-1.64$  eV approximately 1 eV closer to  $E_F$  than the measured value. Another dissimilarity is that the elongated bands originating from the bottom cone have minima midway between  $\bar{\Gamma}_0$  and the surface zone boundary, rather than at the surface zone boundary. In addition, there is an upward degenerate parabolic band at  $\sim -0.1$  eV at  $\bar{\Gamma}_0$ , which is expected to be above  $E_F$  in our measured spectra. All these deviations are likely related to the simplification of the model and the ignoring of the lattice mismatch (2%) between the middle alloy and the bottom Pb(111) film. Due to these deviations, the superimposing of the calculated bands onto the data is made via multiplying the energies of the calculated bands by two plus an offset one for an understandable comparison, as shown in figure 5(h). Nevertheless, a significant outcome of the calculations is that these bands reveal a spin-polarized texture, indicating the time-reversal symmetry to confirm the instinct of the Rashba splitting of these two cones. The downward energy band below the bottom cone with strong  $d$  character of Au is also reproduced with Rashba splitting by calculations. Figure 5(i) displays the calculated contours of the Fermi energy, which substantially resemble the measured ones in figure 2(c); the deeper  $E1$  band and shallower  $E2$  band form the outer and inner hexagonal contours around  $\bar{\Gamma}_0$ , respectively, and the hole pockets around  $\bar{M}$  form two concentric oval contours. Figures 6(a) and (b) show the calculated energy band dispersions in symmetry directions  $\bar{\Gamma}_0 - \bar{M} - \bar{\Gamma}_1$  and  $\bar{\Gamma}_0 - \bar{K} - \bar{M} - \bar{K}$ , respectively, with the dispersion-dependent spin polarizations indicated with red and blue colors. Two Rashba-splitting bands cross at  $-1.73$  eV and  $-2.11$  eV respectively, at  $\bar{M}$ . The former, the top Rashba splitting, clearly exhibits anisotropic Rashba splitting, strong in the direction  $\bar{K} - \bar{M} - \bar{K}$  and weak in the direction  $\bar{\Gamma}_0 - \bar{M} - \bar{\Gamma}_1$ . Gierz *et al* [5] observed such anisotropy in Rashba splitting from a Bi-trimer adlayer on a Si(111) wafer, which breaks the in-plane inversion symmetry along a certain mirror plane; however, the reason for the anisotropy in this case should be different because our calculation considers only a one-layer PbAu alloy with the special buckling. As observed in the side view in figure 5(a), this special buckling also relevantly breaks the in-plane inversion symmetry along the arrow direction, equivalent to  $\bar{K} - \bar{M} - \bar{K}$ , in figure 5(b) possibly due to the strain effect from the Kagome trimers of the capping Au layer, which possess the same asymmetry. The latter, the bottom Rashba splitting, is an extension of the two elongated bands originating from the bottom cone at  $\bar{\Gamma}_0$ . A question that then arises is whether  $\bar{\Gamma}_0$  or  $\bar{M}$ , both time-reversal invariant momenta, is the origin of the Rashba splitting for these elongated bands. Regarding the measured bands in  $\bar{\Gamma}_0 - \bar{M} - \bar{\Gamma}_1$  in figure 2(b), at  $\bar{M}$ , the bottom Rashba splitting is located at  $-3.60$  eV. However, the top Rashba splitting, located at  $-0.94$  eV is too weak to be resolved; only one slightly upward band is hence observed. Figure 6(c) shows the measured energy band dispersions along the direction  $\bar{\Gamma}_1 - \bar{K} - \bar{M} - \bar{K}$ , indicated in figure 2(c), perpendicular to the mirror plane of the photoemission measurement with the  $p$ -polarized synchrotron beam. Their  $k_{\parallel}$  momentum scale is aligned with the calculated ones in figure 6(b) for a detailed comparison. With such a geometric arrangement, the electron states of both even and odd parities are expected to be probed. As observed in figure 6(c), the two elongated bands stemming from the bottom cone at  $\bar{\Gamma}_1$  and going along direction  $\bar{\Gamma}_1 - \bar{K} - \bar{M}$  to form the bottom Rashba splitting at  $\bar{M}$  at  $-3.60$  eV are much better

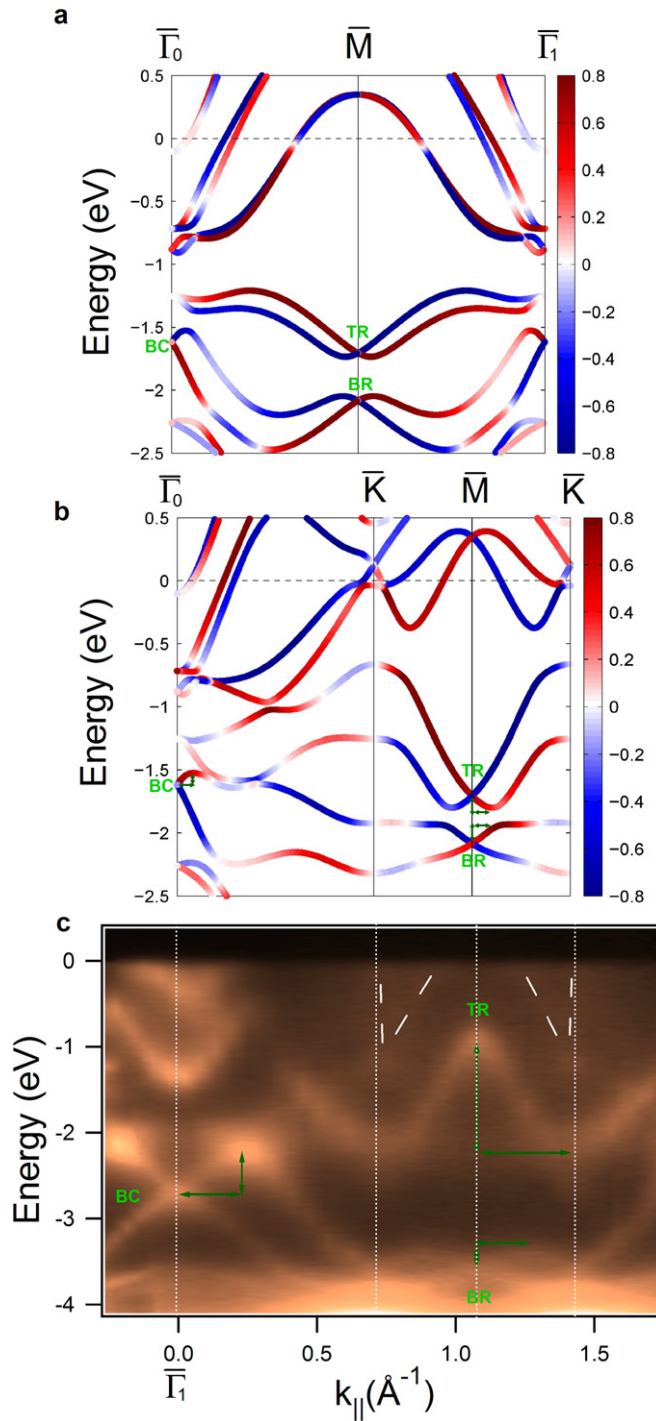


**Figure 6.** (a) Calculated energy band dispersions in the directions  $\bar{\Gamma}_0 - \bar{M} - \bar{\Gamma}_1$  and (b)  $\bar{\Gamma}_0 - \bar{K} - \bar{M} - \bar{K}$ . The red-and-blue scale bar at the right indicates the fraction of opposite spin polarization. (c) Measured band dispersions in the direction  $\bar{\Gamma}_1 - \bar{K} - \bar{M} - \bar{K}$ , which is perpendicular to the mirror plane of the photoemission measurement. Vertical double arrows denote the scales of the Rashba energy  $E_R$  and horizontal arrows for the momentum offset  $K_0$ . The symbols BC, TR, and BR denote the bottom cone, top Rashba splitting and bottom Rashba splitting, respectively.

resolved than in figure 2(a). According to this improved observation, we confirm the calculated result in figure 5(f): the bottom cone at the surface zone center is derived from the Rashba splitting; with the momentum offset  $K_0 = 0.22 \text{ \AA}^{-1}$  and Rashba energy  $E_R = 0.49 \text{ eV}$  the resulting Rashba parameter  $\alpha = \frac{2E_R}{K_0}$  is  $4.45 \text{ eV \AA}$ . The value of the Rashba parameter of the bottom Rashba splitting at  $\bar{M}$  is smaller,  $2.10 \text{ eV \AA}$ ; however, the top Rashba splitting at  $\bar{M}$  at  $-0.94 \text{ eV}$  in this direction again exhibits notable behavior. With  $K_0$  equal to the length  $\bar{K}\bar{M} \sim 0.37 \text{ \AA}^{-1}$  and  $E_R = 1.15 \text{ eV}$  the resulting Rashba parameter  $\alpha_R$  has a value  $6.26 \text{ eV \AA}$ , which is almost twice as large as the value obtained from bulk BiTeI,  $3.8 \text{ eV \AA}$  [34]. The correspondence between the calculation (figure 6(b)) and the measurement (figure 6(c)) for the three key features (bottom cone, top Rashba splitting,

**Table 1.** Rashba parameter  $\alpha_R$  for two cones at  $\bar{\Gamma}_0$  and two Rashba splittings at  $\bar{M}$ .

Rashba parameter/eVÅ	$\bar{\Gamma}_0$		$\bar{M}$			
	Top	Bottom	Top		Bottom	
Measurement	1.53	4.45	$\bar{\Gamma}_0 - \bar{M} - \bar{\Gamma}_1$ $\sim 0$	$\bar{K} - \bar{M} - \bar{K}$ 6.26	$\bar{\Gamma}_0 - \bar{M} - \bar{\Gamma}_1$ 0.41	$\bar{K} - \bar{M} - \bar{K}$ 2.10
Calculation	2.13	3.64	1.46	2.54	1.45	2.55

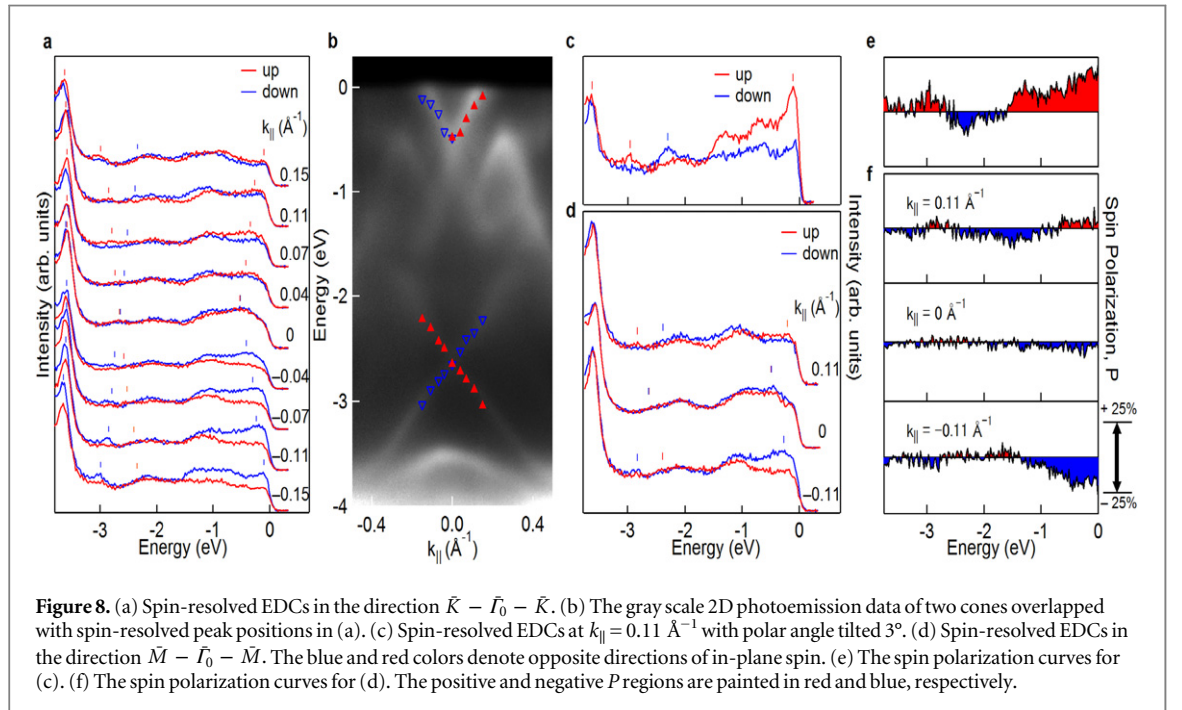
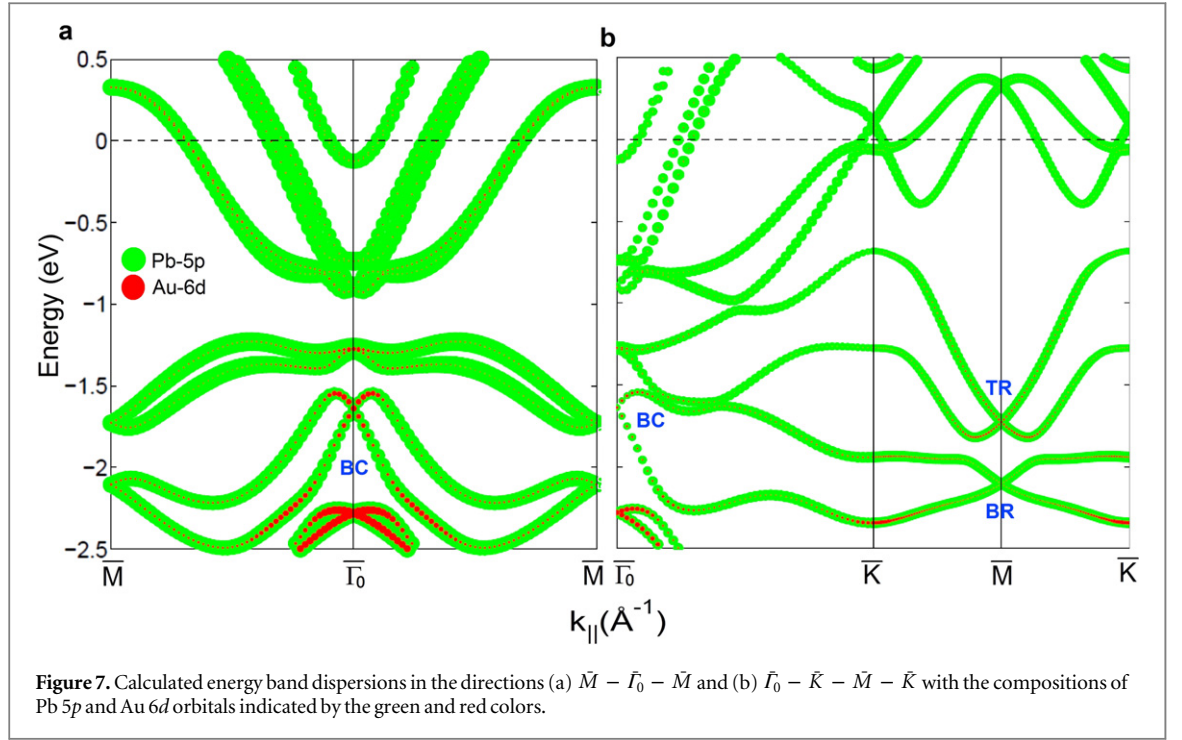
and bottom Rashba splitting) can be understood through the notations BC, TR, and BR, respectively. One can clearly see that the momentum offsets of Rashba splitting,  $K_0$ , for these three features are much larger from the measured data than the calculation, especially for the top Rashba splitting, indicating that the SOC strengths and buckling heights derived from calculation are smaller than the actual counterparts<sup>8</sup>. All the measured and calculated Rashba coupling parameters of the cones at  $\bar{\Gamma}_0$  and the Rashba splitting at  $\bar{M}$  in two symmetry directions are summarized in table 1. Figure 6(c) reveals several other features. Two upward bands across  $E_F$  symmetrical at  $\bar{M}$ , marked with dashed lines for visual guidance, satisfactorily match their spin-polarized counterparts in the calculation in figure 6(b), constituting the bifurcation of the outer and inner ovals centered at  $\bar{M}$ , as observed in figures 2(d) and 5(i). The conspicuously intense upward band at  $\bar{M}$  at  $-2.10$  eV in figure 2(a) is neither observed in figure 6(c) nor reproduced in figure 6(b). We believe that this anomalous band is not inherently derived from the alloy layer but might instead arise from the capping Au Kagome layer or the surface electronic structures of Pb films. The top cone at  $\bar{\Gamma}_1$  in figure 6(c) presents a clear asymmetry—the deeper band at the right and the shallower band at the left, distinct from the case in figure 2(b), in which the top cones appear symmetric.

For clarification, the calculation omits not only the 2% lattice mismatch between the alloy and the underlying Pb films but also the effects, other than strain, of the capping Kagome Au layer, including a charge transfer, interfacial structures and, moreover, the enhanced in-plane anisotropy and observed giant magnitudes of Rashba coupling induced by the Kagome trimers [5, 35]. As observed in table 1, the ratios between the measured Rashba parameters at  $\bar{M}$  in the two symmetry directions are much larger than the calculations, indicating an enhanced anisotropic effect. Interestingly, the outward relaxation of the BiAg-alloy single layer [10, 22] breaks the out-of-plane inversion symmetry but maintains the in-plane inversion symmetry; however, the anisotropic buckling of the single PbAu-alloy layer induced by the top Au Kagome layer and the bottom Pb layers breaks both to cause the anisotropic Rashba splitting at  $\bar{M}$ . It is interesting and reasonable to consider the Rashba effect of this PbAu alloy as the combination of the effects from the BiAg alloy [10] and Bi trimers on Si (111) [5]. Another essential factor for the giant Rashba splitting is the strength of the atomic SOC. In terms of the crystals, Pb 6*p* and Au 5*d* electrons overlap in the energy range about  $-2 \sim -4$  eV so that they have high probabilities of hybridizations between each other around that energy regime. Figures 7(a) and (b) show the calculated energy band dispersions in the directions  $\bar{M} - \bar{\Gamma}_0 - \bar{M}$  and  $\bar{\Gamma}_0 - \bar{K} - \bar{M} - \bar{K}$  with the compositions of Pb 5*p* and Au 6*d* orbitals indicated by the green and red circles whose sizes are proportional to the percentages. As seen, the bands of the bottom cone at  $\bar{\Gamma}_0$  and the top giant Rashba splitting at  $\bar{M}$  contain relevant compositions, 19% and 32%, of Au 5*d* orbitals that possess large spin-orbit splitting of  $\sim 3.8$  eV [36], 2 eV larger than that, 1.8 eV of Pb 6*p* [36]. For the BiAg alloy, the spin-orbit splitting of the Bi 6*p* and Ag 5*p* orbitals are 2.16 eV [36] and 0.11 eV [37], respectively, with a similar large difference of  $\sim 2$  eV. These findings indicate that not only the large SOC strengths of both composite elements [37] but also the difference in the SOC strength between the two hybridized orbitals of the two composite elements is actually an important key, which would cause the large asymmetry of the hybridized wave function, the same effect as the large in-plane potential gradient. In turn, the giant Rashba splitting of the 2D electronic structures occurs because of the hybridizations, regardless of the mass difference between two different composite atoms.

### 3.6. Results of spin-resolved photoemission measurement

Figure 8(a) presents the spin-resolved energy dispersion curves (EDCs) in the direction  $\bar{K} - \bar{\Gamma}_0 - \bar{K}$  for the two cones (top and bottom) near  $\bar{\Gamma}_0$ . The peaks of the top and bottom cones in each pair of EDCs of opposite in-plane spin directions are resolved to show the spin-dependent intensity at each off-normal momentum. The curves follow, moreover, the time-reversal symmetry with respect to  $\bar{\Gamma}_0$ , although the intensity ratio between two opposite spin directions for each pair of EDCs at  $\pm k_{\parallel}$  exhibits an obvious asymmetry due to the effect of spin-dependent dipole matrix elements for photoemission [38]. This trend is more evident for the peaks of the top

<sup>8</sup> As shown in the supplementary material (available at [stacks.iop.org/njp/17/083015/mmedia](http://stacks.iop.org/njp/17/083015/mmedia)), the energy difference between the top Rashba splitting and bottom Rashba splitting at  $\bar{M}$  as well as the momentum offsets of both splitting increase with SO strength and buckling height.



cone near  $E_F$ . The peaks for the bottom cone appear less spin-resolved, especially for the upper half, likely due to interference from other energy bands merely above the bottom cone. With the sample tilted  $3^{\circ}$  in a polar direction, the spin-resolved peaks of the bottom cone become more pronounced in both the upper and lower halves (figure 8(c)). As shown in figure 8(b), the peak positions of spin-polarized EDCs for the two cones are superimposed on the grayscale image of 2D photoemission spectra for clarification. Figure 8(d) presents the spin-resolved EDCs in the direction  $\bar{M} - \bar{\Gamma}_0 - \bar{M}$ , exhibiting the same behavior of time-reversal symmetry for both cones. The corresponding spin polarization curves of the spin-resolved EDCs in figures 8(c) and (d) are exhibited in figures 8(e) and (f), confirming the spin polarizations of the two cones. The peaks below  $-3.50 \text{ eV}$  corresponding to the downward band below the bottom cone also display a Rashba-type spin polarization, consistent with the calculated result in figure 5(f). The calculated spin polarizations of the top cone notably flip

to the opposite in-plane spin directions before crossing  $E_F$ ; the measured spin polarizations of the top cone are consistent with those after flipping in the calculation.

## 4. Conclusion

In conclusion, we discovered a binary-alloy film composed of dual heavy atoms, Au and Pb, which unfolds a large Rashba effect, yielding two cones at  $\bar{\Gamma}_0$  and two giant Rashba splittings at  $\bar{M}$ . Among these effects, the bottom cone at  $\bar{\Gamma}_0$  and the top Rashba splitting at  $\bar{M}$  exhibit great Rashba parameters, 4.45 eVÅ and 6.26 eVÅ, respectively. Calculations of the electronic structure indicate that such a Rashba effect can be produced only via a special buckling configuration induced by squeezing from the top Au and bottom Pb layers. Therefore, unlike the BiAg alloy, whose measured energy bands can be well reproduced by first-principles calculations based on a single freestanding layer of BiAg alloy [22], the theoretical work on this PbAu alloy is more challenging. Despite the inconsistent energy scale, our calculation still reproduced the observed cones and Rashba splitting as well as the spin-polarized contours of the central electron pockets ( $E1$ ,  $E2$ ) around  $\bar{\Gamma}_0$  and the hole pockets ( $H1$ ,  $H2$ ) around  $\bar{M}$ . Therefore the calculation demonstrates the importance of the following contributions, special buckling configuration induced by the strains, and hybridizations of Au  $5d$  and Pb  $6p$  electrons, which might lead to an innovative approach to understanding and tweaking the enhanced Rashba effect of a purely 2D system. For the former, one can use different heavy-element atoms as capping layers to tune the strain on the Rashba effect of the middle alloy, and for the latter, one can further search for other elements with strong SOC of  $d$  orbitals near the Fermi level to develop spintronics driven by  $d$  electrons. Since the discovery of the Rashba effect in BiAg [10], this alloy has served widely as a model for Rashba-type spintronic work [39–43]. This PbAu alloy that we observe is very interesting not just because of even larger Rashba parameter but also its feasibility to exist on a semiconductor. We speculate this to be an alternative system of great significance for the investigation of more advanced development in spintronics, both scientifically and industrially.

## Acknowledgments

The National Science Council of Taiwan (grant NSC 98-2112-M-007-017-MY3 and 102-2112-M-007-009-MY3 to SJT) supported this research. The experiment at the Photon Factory was performed under proposal number 2012G136. HTJ would like to thank NCHC, CINC-NTU and NCTS, Taiwan for technical support. SJT sincerely expresses his gratitude to Juh-Tzeng Lue, who donated many experimental resources, including a piece of Au wire, which yielded the discovery presented in this paper. SJT also thanks T C Chiang for helpful discussion. HL acknowledges the Singapore National Research Foundation for the support under NRF Award No. NRF-NRFF 2013-03.

## References

- [1] Rashba E and Tela F T 1960 *Leningrad* **2** 1224  
Rashba E and Tela F T 1960 *Sov. Phys. Solid State* **2** 1109
- [2] LaShell S, McDougall B A and Jensen E 1996 *Phys. Rev. Lett.* **77** 3419
- [3] Koroteev Y M, Bihlmayer G, Gayone J E, Chulkov E V, Blügel S, Echenique P M and Hofmann P H 2004 *Phys. Rev. Lett.* **93** 046403
- [4] Miyamoto K, Kimura A, Kuroda K, Okuda T, Shimada K, Namatame H, Taniguchi M and Donath M 2012 *Phys. Rev. Lett.* **108** 066808
- [5] Gierz I, Suzuki T, Frantzeskakis E, Pons S, Ostanin S, Ernst A, Henk J, Grioni M, Kern K and Ast C R 2009 *Phys. Rev. Lett.* **103** 046803
- [6] Sakamoto K *et al* 2009 *Phys. Rev. Lett.* **102** 096805
- [7] Yaji K, Ohtsubo Y, Hatta S, Okuyama H, Miyamoto K, Okuda T, Kimura A, Namatame H, Taniguchi M and Aruga T 2010 *Nat. Commun.* **1** 17
- [8] Ohtsubo Y, Hatta S, Yaji K, Okuyama H, Miyamoto K, Okuda T, Kimura A, Namatame H, Taniguchi M and Aruga T 2010 *Phys. Rev. B* **82** 201307
- [9] Höpfner P *et al* 2012 *Phys. Rev. Lett.* **108** 186801
- [10] Ast C R, Henk J, Ernst A, Moreschini L, Falub M C, Pacile D, Bruno P, Kern K and Grioni M 2007 *Phys. Rev. Lett.* **98** 186807
- [11] Pacilé D, Ast C R, Papagno M, Silva C D, Moreschini L, Falub M, Seitsonen A P and Grioni M 2006 *Phys. Rev. B* **73** 245429
- [12] Bihlmayer G, Blügel S and Chulkov E V 2007 *Phys. Rev. B* **75** 195414
- [13] Shanavas K V, Popović Z S and Satpathy S 2014 *Phys. Rev. B* **90** 165108
- [14] Krupin O, Bihlmayer G, Döbrich K M, Prieto J E, Starke K, Gorovikov S, Blügel S, Kevan S and Kaindl G 2009 *New J. Phys.* **11** 013035
- [15] Yu Y, Tang Z, Jiang Y and Fujita D 2008 *Surf. Sci.* **602** 3358
- [16] Qi Y, Yang W, Ma X, Ji S, Fu Y, Zhang Y, Jia J F and Xue Q K 2007 *J. Phys. Condens. Matter* **19** 136005
- [17] Tang S J, Lee C Y, Huang C, Chang T R, Cheng C M, Tsuei K D, Jeng H T, Yeh V and Chiang T C 2011 *Phys. Rev. Lett.* **107** 066802
- [18] Upton M H, Wei C M, Chou M Y, Miller T and Chiang T C 2004 *Phys. Rev. Lett.* **93** 026802
- [19] Perdew J P, Burke K and Ernzerhof M 1996 *Phys. Rev. Lett.* **77** 3865
- [20] Blöchl P E 1994 *Phys. Rev. B* **50** 17953
- [21] Kresse G and Hafner J 1993 *Phys. Rev. B* **48** 13115
- [22] Bian G, Wang X, Miller T and Chiang T C 2013 *Phys. Rev. B* **88** 085427
- [23] Gierz I, Stadtmüller B, Vuorinen J, Lindroos M, Meier F, Dil J H, Kern K and Ast C R 2010 *Phys. Rev. B* **81** 245430

- [24] Höpfner P *et al* 2011 *Phys. Rev. B* **83** 235435
- [25] Nakatsuji K, Niikura R, Shibata Y, Yamada M, Iimori T and Komori F 2011 *Phys. Rev. B* **84** 035436
- [26] Upton M H, Miller T and Chiang T C 2005 *Phys. Rev. B* **71** 033403
- [27] Dil J H, Kim J W, Kampen T, Horn K and Ettema A R H F 2006 *Phys. Rev. B* **73** 161308
- [28] Zhang Y, Tan Y W, Stormer H L and Kim P 2005 *Nature* **438** 201
- [29] Chen Y L *et al* 2009 *Science* **325** 178
- [30] Fu L 2009 *Phys. Rev. Lett.* **103** 266801
- [31] Perltz H 1934 *Tartu RiiklikuUlik. Toim.* **27** 3–15
- [32] Lin C H, Berlin T, Wang L, Lee C C, Yin W G and Ku W 2011 *Phys. Rev. Lett.* **107** 257001
- [33] Mans A *et al* 2006 *Phys. Rev. Lett.* **96** 107007
- [34] Ishizaka K *et al* 2011 *Nature Mater.* **10** 521
- [35] Frantzeskakis E, Pons S and Grioni M 2010 *Phys. Rev. B* **82** 085440
- [36] Ley L, Kowalczyk S P, McFeely F R and Shirley D A 1974 *Phys. Rev. B* **10** 4881
- [37] Moreschini L, Bendounan A, Bentmann H, Assig M, Kern K, Reinert F, Henk J, Ast C R and Grioni M 2009 *Phys. Rev. B* **80** 035438
- [38] Jozwiak C *et al* 2011 *Phys. Rev. B* **84** 165113
- [39] Rojas Sánchez J C *et al* 2013 *Nat. Commun.* **4** 2944
- [40] Hirayama H, Aoki Y and Kato C 2011 *Phys. Rev. Lett.* **107** 027204
- [41] Cottin M C, Lobo-Checa J, Schaffert J, Bobisch C A, Möller R, Ortega J E and Walter A L 2014 *New J. Phys.* **16** 045002
- [42] He K *et al* 2010 *Phys. Rev. Lett.* **104** 156805
- [43] Bian G, Zhang L, Liu Y, Miller T and Chiang T C 2012 *Phys. Rev. Lett.* **108** 186403